An Electron-Stimulated Desorption Ion Angular Distribution and Low-Energy Electron Diffraction Investigation of CF_3I on Ru(001)

M. B. Jensen, J. S. Dyer,† W.-Y. Leung, and P. A. Thiel*

Department of Chemistry and Ames Laboratory, Iowa State University, Ames, Iowa 50011

Received March 17, 1995. In Final Form: November 28, 1995⊗

We have investigated the structures of CF_3I, and its dissociation products, adsorbed on Ru(001) using low-energy electron diffraction and electron-stimulated desorption ion angular distribution (ESDIAD). Atomic iodine forms $(\sqrt{3}x\sqrt{3})R30°$ islands even at very low coverages. At 70% of saturation and above, a (2×2) superstructure forms which we attribute to a $p(2\times2)$ unit cell with one CF_3 group and one iodine atom. ESDIAD images show F^+ desorbing at normal emission and in three hexagonal patterns. The normal emission is attributed to a tilted configuration of CF_3(ad) in which one C−F bond is oriented perpendicular to the surface. A small hexagon is attributed to F(ad) on step edges. A large hexagon at low coverages may arise from isolated CF_3(ad) species possessing C_{3v} symmetry. And finally, an intermediate hexagon is attributed to perturbation of the CF_3(ad) orientation by molecular fragments which result from electron irradiation of physisorbed CF_3I.

1. Introduction

The widespread use of fluorocarbons in technical applications has generated much interest in the chemistry of these molecules adsorbed on surfaces. In particular, the chemistry of trifluoroiodomethane (CF_3I) adsorbed on metal surfaces has been the subject of several recent investigations.[1−8] The relatively weak C−I bond (2.3 eV) is easily cleaved thermally, making CF_3I an ideal precursor for examining the reactivity of adsorbed trifluoromethyl groups—just as a number of studies have successfully utilized iodoalkanes as precursors to adsorbed alkyl groups.[9]

While a number of surface-sensitive experimental techniques have been applied to the study of adsorbed CF_3I, electron-stimulated desorption ion angular distribution (ESDIAD) is one technique yet to be utilized. Fluorine-containing compounds are ideal for investigation with techniques based on electron-stimulated desorption (ESD) due to the high ESD cross section of F^+.[10,11] This sensitivity, coupled with the strong possibility of azimuthal ordering of CF_3(ad) on a close-packed surface, makes CF_3I on Ru(001) an ideal system for ESDIAD analysis. ESDIAD has been applied previously to the study of other highly-symmetric, fluorine-containing compounds adsorbed on metals, notably NF_3 on Ru(001),[12] SF_6 on W(011) and W(111),[13] and PF_3 on Ni(111)[14,15] and Ru(001).[16−21] We also note a recent related study of the ESDIAD behavior of CCl_4 on Ru(001).[22] To our knowledge, however, ESDIAD has yet to be applied to the investigation of an adsorbed fluorocarbon.

Table 1. Summary of TDS Results (Reference 2)

desorbing species	peak temperature (K)	onset exposure (% saturation)	exposure at maximum yield (% saturation)
I	1130−1060	0	100
F	270−390	18	100
	1226	24	67
CF_3I	145	18	100
	136	100	n/a
CF_2	1165	44	71
CF_3	705	67	100
CF_4	605	100	100

In this paper we present the results of an ESDIAD investigation of CF_3I on Ru(001). The results of a previously reported thermal desorption spectroscopy (TDS) study of CF_3I on Ru(001) are summarized in Table 1.[2] Desorption states attributable to CF_3I, CF_4, CF_3, CF_2, F, and I were identified. While this product distribution revealed that C−F and C−I bonds must break, it did not serve to identify the associated adsorbed species.

Hence, a second study was undertaken to identify surface adsorbates, utilizing X-ray photoelectron spec-

† Current address: Space Dynamics Laboratory, Utah State University, Logan, Utah 84321-1942.

⊗ Abstract published in *Advance ACS Abstracts,* June 1, 1996.

(1) Jones, R. G.; Singh, N. K. *Vacuum* **1988**, *38*, 213.
(2) Dyer, J. S.; Thiel, P. A. *Surf. Sci.* **1990**, *238*, 169.
(3) Liu, Z.-M.; Zhou, X.-L.; Kiss, J.; White, J. M. *Surf. Sci.* **1993**, *286*, 233.
(4) Castro, M. E.; Pressley, L. A.; Kiss, J.; Pylant, E. D.; Jo, S. K.; Zhou, X.-L.; White, J. M. *J. Phys. Chem.* **1993**, *97*, 8476.
(5) Armentrout, D. D.; Grassian, V. H. *Langmuir* **1994**, *10*, 2071.
(6) Sun, Z.-J.; Schwaner, A. L.; White, J. M. *Chem. Phys. Lett.* **1994**, *219*, 118.
(7) Jensen, M. B.; Myler, U.; Jenks, C. J.; Pylant, E. D.; White, J. M.; Thiel, P. A. *J. Phys. Chem.* **1995**, *99*, 8736.
(8) Jensen, M. B.; Thiel, P. A. *J. Am. Chem. Soc.* **1995**, *117*, 438.
(9) Zaera, F. *Acc. Chem. Res.* **1992**, *25*, 260.
(10) de Moraes, M.; Lichtman, D. *J. Vac. Sci. Technol., A* **1984**, *2*, 1595.
(11) de Moraes, M.; Lichtman, D. *Surf. Sci.* **1985**, *160*, 362.
(12) Walczak, M. M.; Johnson, A. L.; Thiel, P. A.; Madey, T. E. *J. Vac. Sci. Technol., A* **1988**, *6*, 675.
(13) Madey, T. E.; Yates, J. T., Jr. *Surf. Sci.* **1977**, *63*, 203.
(14) Alvey, M. D.; Yates, J. T., Jr.; Uram, K. J. *J. Chem. Phys.* **1987**, *87*, 7221.
(15) Alvey, M. D.; Yates, J. T., Jr. *J. Am. Chem. Soc.* **1988**, *110*, 1782.
(16) Joyce, S. A.; Johnson, A. L.; Madey, T. E. *J. Vac. Sci. Technol., A* **1989**, *7*, 2221.
(17) Joyce, S. A.; Yarmoff, J. A.; Madey, T. E. *Surf. Sci.* **1991**, *254*, 144.
(18) Joyce, S. A.; Clark, C.; Chakarian, V.; Shuh, D. K.; Yarmoff, J. A.; Madey, T. E.; Nordlander, P.; Maschhoff, B.; Tao, H.-S. *Phys. Rev. B* **1992**, *45*, 14264.
(19) Johnson, A. L.; Joyce, S. A.; Madey, T. E. *Phys. Rev. Lett.* **1988**, *61*, 2578.
(20) Madey, T. E.; Joyce, S. A.; Yarmoff, J. A. In *Chemistry and Physics of Solid Surfaces VIII*; Vanselow, R., Howe, R., Eds.; Springer-Verlag: Berlin, 1990; Vol. 22; p 55.
(21) Madey, T. E.; Nair, L.; Diebold, U.; Shivaprasad, S. M.; Johnson, A. L.; Poradzisz, A.; Shinn, N. D.; Yarmoff, J. A.; Chakarian, V.; Shuh, D. In *Desorption Induced by Electronic Transitions DIET V*; Burns, A. R., Stechel, E. B., Jennison, D. R., Eds.; Springer-Verlag: Berlin, 1993; Vol. 31; p 182.
(22) Sack, N. J.; Nair, L.; Madey, T. E. *Surf. Sci.* **1994**, *310*, 63.

S0743-7463(95)00211-3 CCC: $12.00

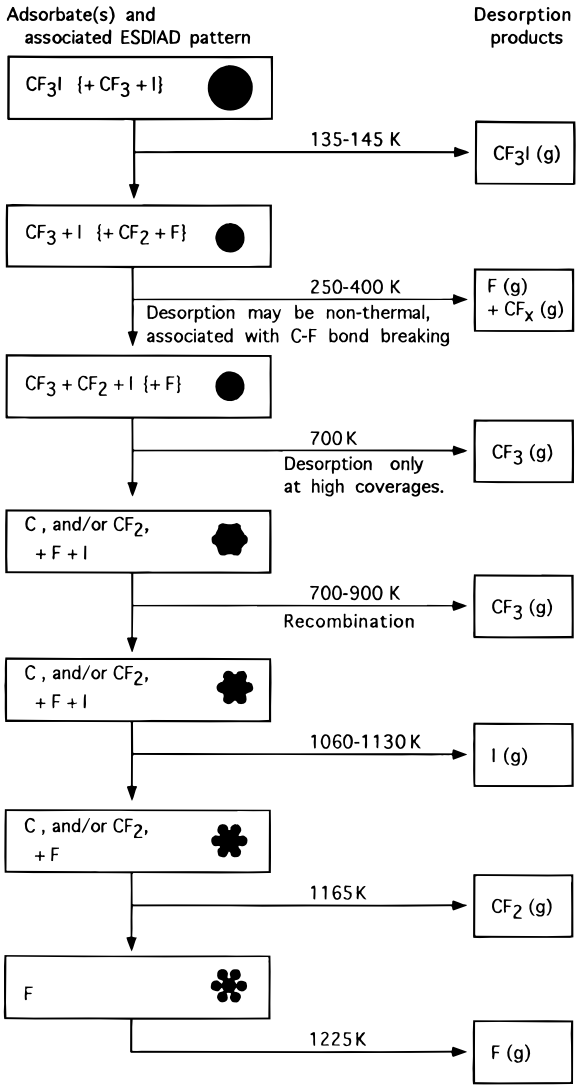

Figure 1. Schematic representation of surface adsorbates, gas-phase desorbates, and ESDIAD patterns produced for CF_3I on Ru(001), starting from (at top) saturation or above-saturation exposure at 100 K. The temperatures given are peak temperatures of desorption states, except for the CF_3(g) produced by recombination, where a peak does not exist and an entire range of temperatures is given over which this product forms. Minority species are listed in brackets.

troscopy (XPS), high resolution electron energy loss spectroscopy (HREELS), and H_2 coadsorption results, as well as preliminary ESDIAD data.[7] The model which emerged from this study is summarized in Figure 1. Adsorption of CF_3I at 100 K is both molecular and dissociative, resulting in CF_3I(ad), CF_3(ad), and I(ad). By 200 K all C−I bonds are broken and some CF_3(ad) is decomposed to CF_2(ad). Between 200 and 400 K, in a process at least partially induced by H(ad) from background H_2 adsorption, further defluorination of CF_3 occurs. At high coverages, surface fragments combine at 605 K to desorb as CF_4, followed by desorption of CF_3, peaking at 705 K. As CF_3 desorption proceeds, surface sites are opened up for further decomposition of CF_3, and possibly CF_2. Some of these fragments recombine below 900 K and desorb as CF_3. HREELS, in conjunction with ESDIAD, indicated that the CF_3(ad) species is tilted, with one C−F bond oriented normal to the surface plane.

In the current paper, we present the full results of the ESDIAD study, along with low-energy electron diffraction (LEED) results, covering the entire range of coverage and temperature following CF_3I adsorption at 100 K. Our goal is to probe the short- and long-range structures of the adsorbates identified previously.

2. Experimental Details

The experiments are performed in a stainless steel, ultrahigh vacuum (UHV) chamber with a base pressure of 8×10^{-11} Torr. The chamber, described previously,[23] is equipped for TDS, ESDIAD/LEED, Auger electron spectroscopy (AES), ion bombardment, and gas introduction.

ESDIAD and LEED experiments are carried out using an optics assembly consisting of three wire mesh grids (two hemispherical and one planar) followed by a dual microchannel plate (MCP) assembly and a phosphor-coated viewing screen. The electron source is a PHI Model 04-015 grazing incidence electron gun. Images are monitored with a CCD video camera and recorded with a videocasset recorder. All ESDIAD and LEED images shown in this report are photographed from videotape, although both live and recorded images may be digitized using a HP Vectra QS/20 computer equipped with a video processor board (Matrox MVP-AT).

A primary electron beam energy set at 250 eV, with a sample current of 25 nA, is used in the ESDIAD experiments. By focusing the electron beam on a phosphor-coated aluminum flag, we estimate the beam diameter at approximately 1 mm, resulting in an electron flux of 2×10^{11} s^{-1} mm^{-2}. An image compression bias of +30 V is applied to the crystal, resulting in a net primary beam energy of +280 eV. The mesh grid closest to the crystal is held at ground potential, the second at +34 V, and the third at −300 V. The first grid serves to accelerate the positive ions and to filter out electrons, the second to filter out positive ions with low kinetic energy, and the third to accelerate the positive ions again. All ESDIAD images are taken at $T \leq 170$ K after heating the crystal to the desired temperature; the ESDIAD images are invariant with temperature below 170 K. The electron beam may be rastered with the electron gun deflection plates to avoid excessive electron beam damage. The incident electron beam strikes the sample about 75° from the surface normal, while the sample surface is perpendicular to the central axis of the ESDIAD optics.

Ideally, one could determine the desorption angles corresponding to off-normal emission in ESDIAD by rotating the zero-biased crystal under the electron beam until a lobe is positioned in the middle of the phosphor screen. This would provide information about adsorbate bond angles. Unfortunately, the design of our cryogenic cold finger, in which the sample does not fall on or near a rotational axis, makes this impossible.

LEED experiments are performed using the same gun and optics, and sample geometry, as for ESDIAD. The beam energy is 250 eV and the current from sample to ground is 40 nA, yielding an electron flux of 3×10^{11} s^{-1} mm^{-1}. The sample and the first grid are tied at ground. The second grid is at −230 V, and the third at 0 V. These grids serve the same purpose as in any standard LEED optics.[24] The microchannel plates are typically biased at +254, +773, and +1265 V, going from the grid side to the window side. Observations are recorded at $T \leq 170$ K, a range where temperature has no effect.

TDS experiments are performed using a UTI 100C quadrupole mass spectrometer (QMS) interfaced to an HP Vectra QS/20 computer for simultaneous monitoring of one to eight masses. A series of three electrostatic lenses, with 8 mm circular apertures, shield the crystal from stray electron current from the QMS ionizer during the TDS experiment.[2] Biasing voltages of 0, −55, and +2 V (with 0 nearest the sample) provide sample currents in the nanoampere range, when the sample is at ground. The sample surface is perpendicular to the axis of the ionizer and quadrupole and is in direct line-of-sight.

The QMS is also used to identify ions generated by ESD. In such an experiment, the sample geometry is the same as that for TDS, and a second electron gun supplies a beam at grazing incidence. The QMS ionizer is off. The beam energy is 250 eV, the crystal bias is +32 V, and the three lenses are biassed at −3, −12, and 0 eV. The beam current is approximately 300 nA.

(23) Walczak, M. M.; Thiel, P. A. *Surf. Sci.* **1989**, *224*, 425.
(24) Ertl, G.; Kuppers, J. In *Low Energy Electrons and Surface Chemistry*; VCH Verlagsgesellschaft: Weinheim, 1985.

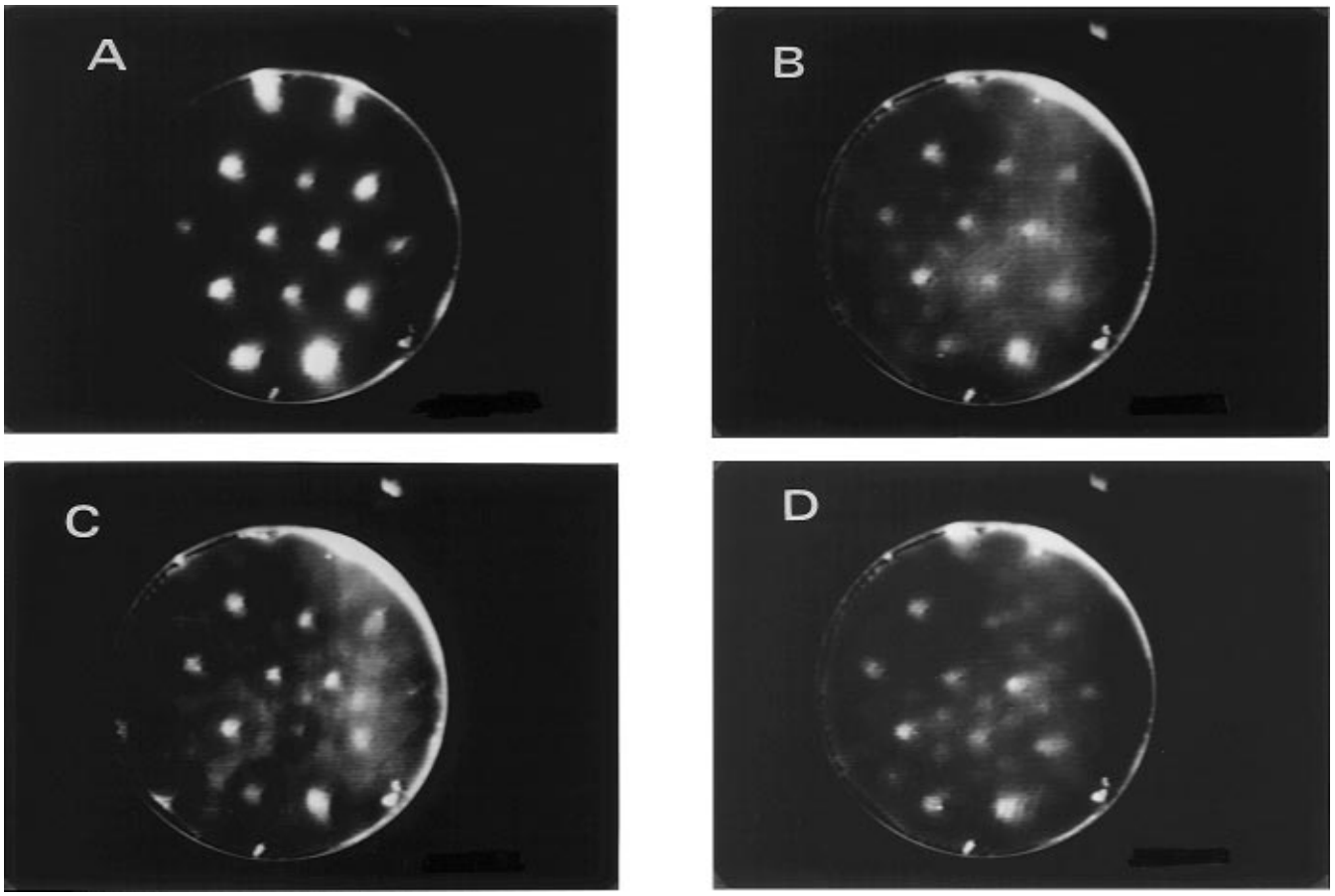

Figure 2. LEED patterns resulting from a saturation exposure of CF_3I on Ru(001): (A) (1×1) from the clean surface; (B) p(2×2) resulting from heating to 400 K; (C) splitting of the p(2×2) following heating to 700 K; (D) $(\sqrt{3}\times\sqrt{3})R30°$ visible upon heating to 800 K.

In some cases, the crystal is flooded deliberately with low-energy electrons from the ionizer of the QMS. The current density is 5×10^{12} s^{-1} mm^{-2}, and the maximum electron energy is 110 eV. The temperature of the crystal rises by no more than 5 K during such irradiation.

The Ru(001) single crystal is spot welded to two Ta rods in thermal contact with a liquid-nitrogen-coolable cold finger. This configuration allows for resistive heating to 1700 K, followed by rapid cooling to 100 K. Temperature is monitored with a W 5% Re−W 26% Re thermocouple spotwelded to the back of the crystal. In thermal desorption, the heating rates in specific temperature ranges are 5 K/s (100−250 K), 2 K/s (250−400), and 4 K/s (400−1600 K). The rate is accelerated deliberately at 400 K to speed up the experiment and improve signal-to-noise. The deceleration at 250 K is an artifact of the temperature feedback circuit. Cooling from 1700 to 100 K occurs in about 5 min.

The Ru(001) sample, about 1 cm^2 in area and 1.2 mm thick, is grown at the Materials Preparation Center of the Ames Laboratory. It is oriented and polished to within ±1° of the (001) face on both sides.[23] Major contaminants in the freshly-cut crystal were carbon, oxygen, and silicon. These were removed by a combination of argon ion bombardment, oxygen exposure, and annealing, with surface cleanliness monitored by AES. Subsequently, carbon (undetectable by AES in small amounts due to overlap with a Ru transition) was removed by oxygen titration: small oxygen exposures at room temperature or below were followed by measurements of CO desorption, until the CO yield was immeasurable.[23] Eventually, a simpler procedure was developed, which also gave a clean surface reproducibly. This consisted of exposure to 5−10 langmuirs of O_2 at 700 K followed by annealing at 1700 K to remove residual oxygen. The sample is cleaned between experiments in this fashion, and exhibits a sharp p(1×1) pattern in LEED.

Ion bombardment is carried out by bleeding Ar continuously through the chamber and out through a 170 L/s Balzer's turbomolecular pump, maintaining a steady-state pressure of 10^{-6} Torr. Sputtering is typically carried out in 15-min periods. Traces of oxygen are detectable with AES after sputtering. On Ni, identical sputtering conditions leave detectable but small amounts of carbon as well. The Ar purity is specified by the vendor as 99.998%.

CF_3I is purchased from PCR, Inc., which specifies 99.0% purity. Further purification is accomplished by several freeze−pump−thaw cycles with liquid nitrogen. XeF_2 is purchased from Aldrich. Transfer of the XeF_2 to a sealed glass vial with vacuum fittings is carried out in a helium-filled glovebox. Both CF_3I and XeF_2 are introduced into the vacuum chamber through an all-metal, directional gas doser connected to a gas-handling manifold.[23] The sample is perpendicular to the axis of the doser and is about 5 mm away. The background pressure rises typically by 1×10^{-10} Torr during dosing. Exposures of CF_3I are given in percentages of the exposure necessary to saturate the first layer. Saturation is taken as the point where the yield of gas-phase, atomic iodine reaches a plateau as a function of increasing CF_3I exposure.[2] Yields of iodine and other species are measured by integrating thermal desorption peak areas.

3. Results

3.1. LEED. Figure 2 illustrates all of the LEED patterns which occur in this system. The (1×1) pattern obtained from the clean surface is shown in Figure 2A. The remainder of the figure shows results after annealing a multilayer coverage. Superstructures develop well after desorption of the multilayer state itself (Table 1); Figure 2B shows that half-order spots appear after annealing to 400 K. Increasing the temperature to 700 K causes these nonintegral spots to split, as shown in Figure 2C. This splitting yields the $(\sqrt{3}\times\sqrt{3})R30°$ pattern seen in Figure 2D, upon annealing to 800 K. At 1100 K only the (1×1) spots remain.

As for the coverage dependence of the LEED patterns, only the (1×1) is seen for exposures below 20% saturation.

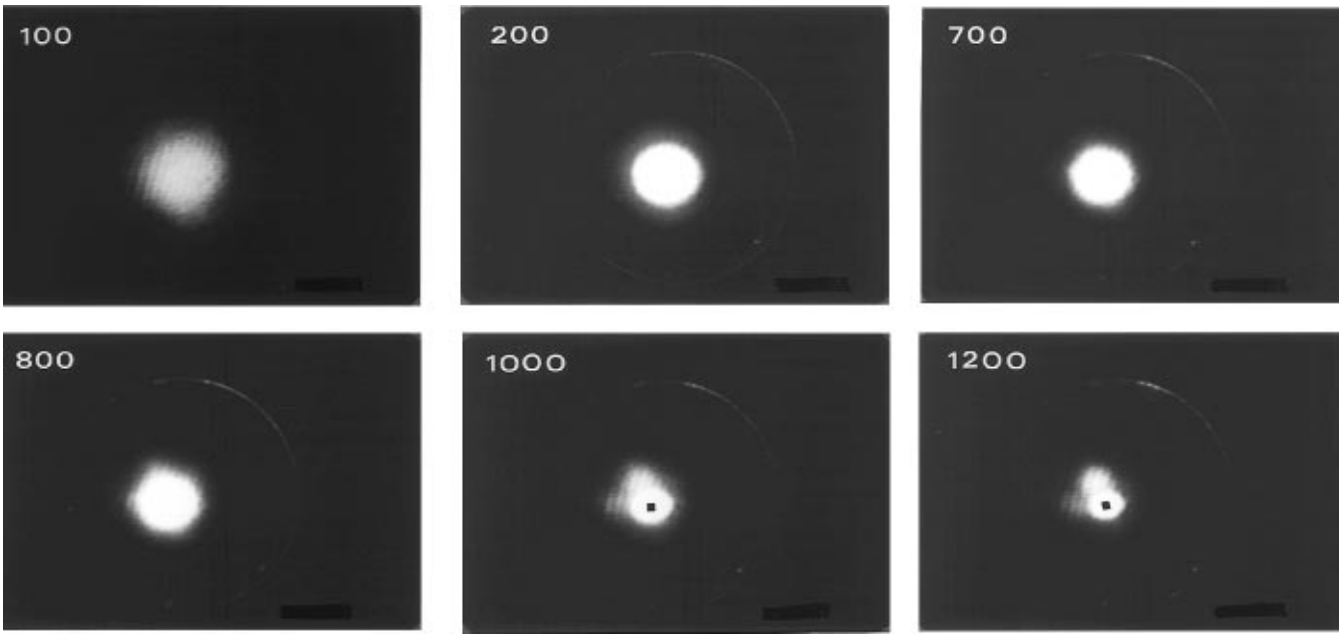

Figure 3. ESDIAD images shown for a multilayer exposure of CF_3I as a function of temperature.

From 20% to 70% saturation, the $(\sqrt{3}x\sqrt{3})R30°$ pattern emerges between 300 and 600 K. In this coverage regime the temperature of first appearance of the $\sqrt{3}$ pattern decreases with increasing coverage, but its disappearance is always complete by 1100 K. The LEED pattern showing 1/2 order beams first appears at approximately 70% saturation, where the CF_3 desorption state also emerges (Table 1), and is visible at all exposures thereafter. These 1/2 order beams appear at 300 K, begin to split at 500 K, and disappear at 800 K, leaving the $\sqrt{3}$ pattern, which once again is gone by 1100 K.

3.2. ESDIAD. The identities of the positive ion products resulting from electron-stimulated desorption (ESD) are determined by focusing the desorbing species into the QMS with the ionizer current turned off. At all exposures and temperatures examined, F^+ is the dominant ESD product. Minor contributions from CF_n^+ species are observed, especially upon electron irradiation of the condensed multilayer. No I^+ is ever detected, suggesting that iodine does not undergo ESD. This is corroborated by the fact that the iodine concentration, as measured by AES, remains constant during electron irradiation by the Auger beam. More specifically, the I(511)/Ru(273) AES ratio shows no decline over 30 min of continuous electron irradiation (2250 eV, 4 μA sample current) following a 75% saturation exposure of CF_3I at 100 K. On the basis of these observations, we interpret all ESDIAD images as being generated by ESD of F^+.

Figure 3 illustrates the temperature dependence of the ESDIAD images which can result from a multilayer CF_3I exposure. Following adsorption at 100 K, a broad, diffuse image is generated, attributable to a disordered multilayer. Following heating to 200 K, which results in desorption of both physisorbed and chemisorbed molecular CF_3I (Table 1), the corresponding ESDIAD image is a circular spot, much sharper and more focused than in the 100 K case, indicating emission of F^+ normal to the crystal surface. This normal emission image remains unchanged until 700 K, when the lobes of a small hexagonal pattern begin to emerge beneath the strong center beam. These lobes become more distinct at 800 K.

Heating to 1000 K results in a decrease in the normal emission intensity, thereby making the lobes of the small hexagon still more visible. While the 1000 K photograph presented in Figure 3 shows only two of these lobes clearly, rastering the incident electron beam over the entire crystal surface reveals all six lobes, although rarely at the same time. Even when more than two are visible, the same two lobes are always most intense. After heating to 1200 K, the central spot and small hexagon are still visible, but with lower intensity. In this case, rastering the electron beam shows regions where all six lobes of the hexagon are plainly seen, but with no central spot. All ESDIAD features disappear by 1250 K.

The progression of the small hexagon and central spot depends upon coverage. First, consider the advent of the small hexagon. While this pattern is first visible at 700 K after a multilayer CF_3I exposure (Figure 3), it is observed at lower temperatures for lower exposures. For instance, Figure 4A shows the ESDIAD image produced after heating a 30% saturation exposure to 400 K. Two somewhat-unresolved lobes of the small hexagon are visible already at this temperature, along with a small normal emission spot. (At low exposures, the advent of the small hexagon at 400 K is always accompanied by a visible decrease in the normal emission intensity; this correlation may hold as well at higher coverage, but is difficult to discern due to the very high intensity of the central spot.) A second coverage-dependent event is the disappearance of the central spot, accompanied or followed by disappearance of the hexagon. The central spot for the 30% saturation exposure disappears in some areas at 1100 K, with the entire image gone by 1150 K; entire disappearance occurs only at 1250 K for the multilayer.

Also visible at low CF_3I exposures, albeit faintly, is a large hexagonal pattern, shown in Figure 5 for a 30% saturation exposure flashed to 500 K. (The small hexagon is unresolved due to the high channel plate gain.) This large hexagon is visible from the lowest exposures through approximately 50−60% saturation exposure, first appearing at 400 K and disappearing by 600−700 K for all these exposures. If a CF_3I exposure below 50% saturation is flashed directly to 500 K after dosing, this image is immediately visible over the entire crystal surface, suggesting that the pattern develops at low exposures without electron irradiation. However, as the exposure approaches saturation, this large hexagon becomes visible only with increasing electron fluence. This suggests that the species responsible for the large hexagon develops at low exposures

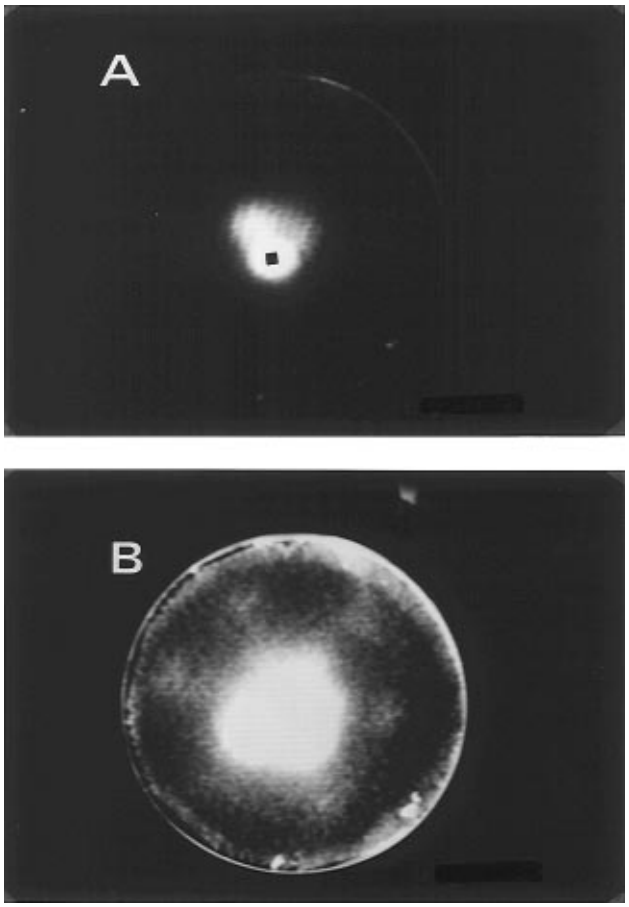

Figure 4. ESDIAD images: (A) two lobes of the small hexagon, plus normal emission, obtained after exposing to 30% of saturation and heating to 400 K; (B) as in (A), but the MCP gain is increased to reveal the large hexagon.

only via thermal activation, but is assisted at high exposures by electron activation.

A similar large hexagon is visible with the electron beam focused on the crystal edge, a photograph of which appears in ref 7. This pattern is visible at all CF_3I exposures, appearing at 200 K for low exposures and at 400 K for exposures closer to, or exceeding, saturation. Regardless of exposure, this pattern from the crystal edge disappears by 800 K.

3.3. Defect-Related Chemistry. Much information can be gained regarding the influence of defect sites on the CF_3I chemistry by ion bombarding the crystal surface prior to adsorption. Of particular interest is the effect of defect sites on the observed ESDIAD images. In our experiments, a "defect-rich" surface is prepared by Ar^+ sputtering for 15 min followed by annealing to 700 K to desorb residual background gases and embedded Ar. According to AES (section 2), this surface contains traces of carbon and oxygen. The resulting LEED pattern shows (1×1) spots on a diffuse background. CF_3I is then adsorbed at 100 K.

As demonstrated in Figure 5, the thermal chemistry of CF_3I is much different on such a surface. Curve a shows the CF_3^+ TDS signal following multilayer adsorption on a well-annealed surface. The result is similar to that reported previously.[2] The main feature is a CF_3 desorption state at 705 K. (Smaller features at 510 and 590 K in curve a are due to electron beam damage, as discussed below, while the feature visible at 420 K is a result of desorption from the Ta supports following an abrupt increase in the heating rate at this temperature. If the heating rate is maintained constant in this temperature

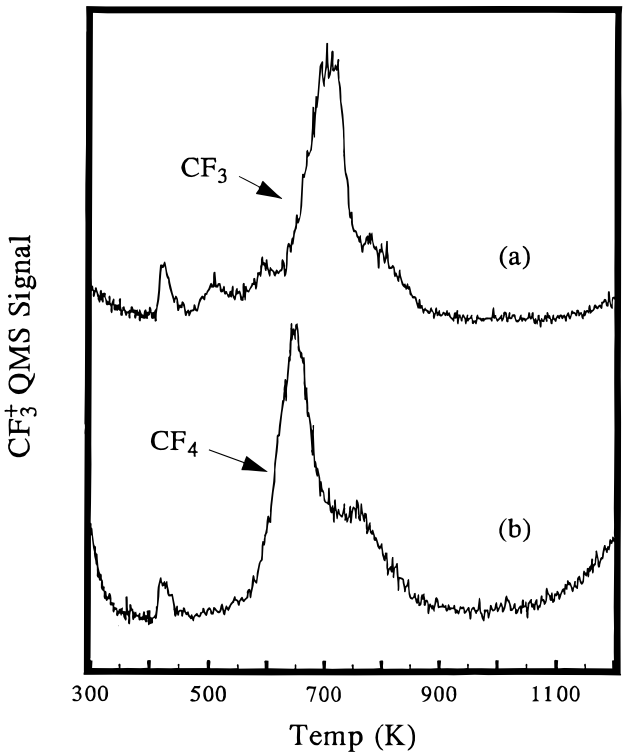

Figure 5. TDS signal for CF_3^+ resulting from a saturation exposure of CF_3I at 100 K onto (a) clean, well-annealed Ru(001) and (b) Ar^+ sputtered Ru(001) annealed to 700 K.

regime, no such feature is observed.) Curve b shows the same result when a defect-rich surface is used. Curve b at first appears to show only a downward temperature shift of the features in curve a. However, examination of the cracking pattern (especially the CF^+ and CF_2^+ intensities[2]) in the same temperature region (not shown) shows that the large peak at 650 K is now actually CF_4, not CF_3! (CF_4 desorption had been previously observed as a minor desorption product at this same temperature.[2]) The high-temperature foot in curve b, which extends to approximately 900 K, remains as CF_3.

Figure 6A shows the ESDIAD pattern observed after the surface is exposed to 20% saturation CF_3I on a defect-rich surface and then heated to 500 K. All six lobes of the small hexagon are now visible, with no central beam. The image does not change as the electron beam is rastered across the surface. A similar pattern is seen from all exposures up through saturation on the defect-rich surface, although as the exposure increases, the normal emission beam returns and intensifies. The large hexagonal pattern described above is seen also at all CF_3I exposures on the defect-rich surface, but *only* on the edges of the crystal.

In an attempt to examine ESDIAD images generated by atomic fluorine, we turn to experiments involving adsorption of XeF_2. XeF_2 has previously been utilized as a source of atomic fluorine on metal surfaces.[25] Figure 6B shows the ESDIAD image following exposure of XeF_2 onto a defect-rich surface at 300 K. A small hexagon, identical to that shown in Figure 6A, is observed.

3.4. Electron-Induced Chemistry. Great care must be taken in ESDIAD experiments to distinguish between those features which reflect the intrinsic surface geometry of the adsorbate and those which are artifacts of electron-induced chemistry. A good example is provided by the present system.

(25) Loudiana, M. A.; Dickinson, J. T.; Schmid, A.; Ashley, E. J. *Appl. Surf. Sci.* **1987**, *28*, 311.

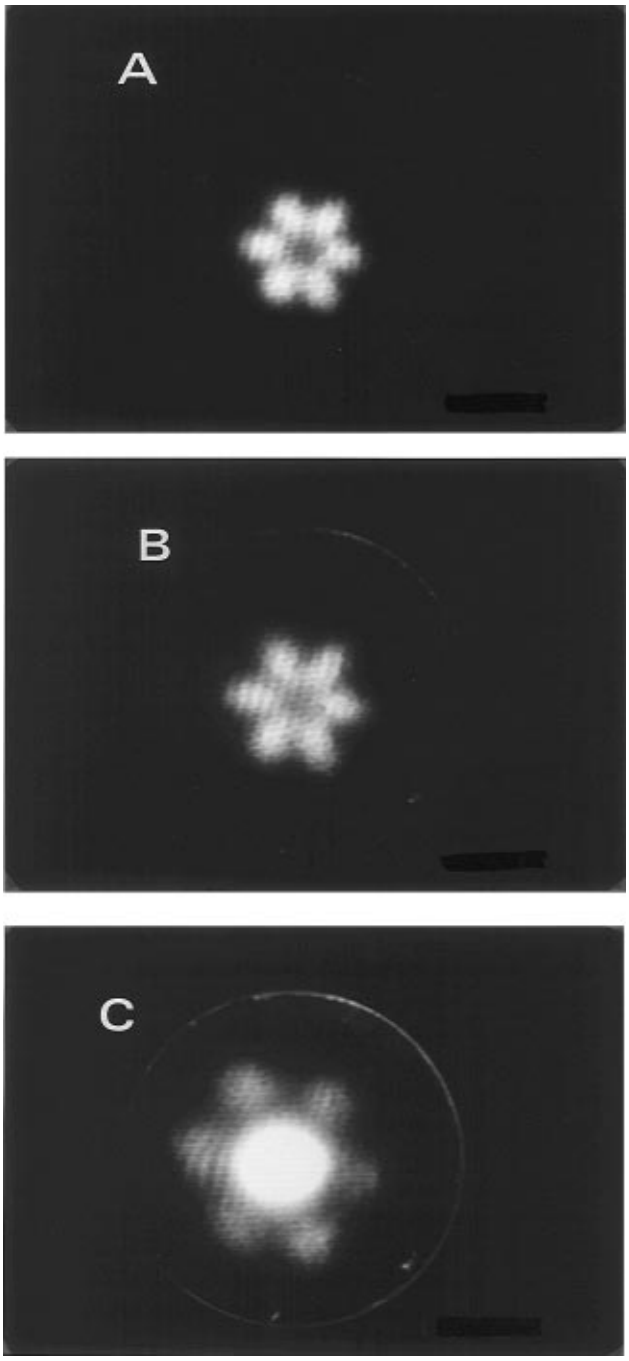

Figure 6. ESDIAD images: (A) all six lobes of the small hexagon after a 20% saturation CF_3I exposure at 100 K onto an Ar^+ sputtered, partially annealed surface, the particular image shown here follows heating to 500 K; (B) image resulting from XeF_2 exposure at 300 K onto an Ar^+ sputtered, partially annealed Ru(001) surface, the image is obtained after heating to 500 K; (C) intermediate hexagon which results from electron irradiation of multilayer CF_3I following adsorption at 100 K, the image shown is following heating to 500 K.

If, following a multilayer CF_3I exposure on an annealed surface, one spot of the crystal is irradiated for an extended period of time with the focused electron beam and then annealed, the ESDIAD images from that spot contain a new pattern. This pattern, shown in Figure 6C for a multilayer exposure heated to 500 K following 5 min of electron bombardment, is a hexagonal image intermediate in size to the small hexagon of Figure 6A and the large hexagon of Figure 4B. This intermediate hexagon is first visible at 400 K, disappearing by 700 K.

The entire crystal surface may be irradiated with low-energy electrons by placing a positive bias on the crystal

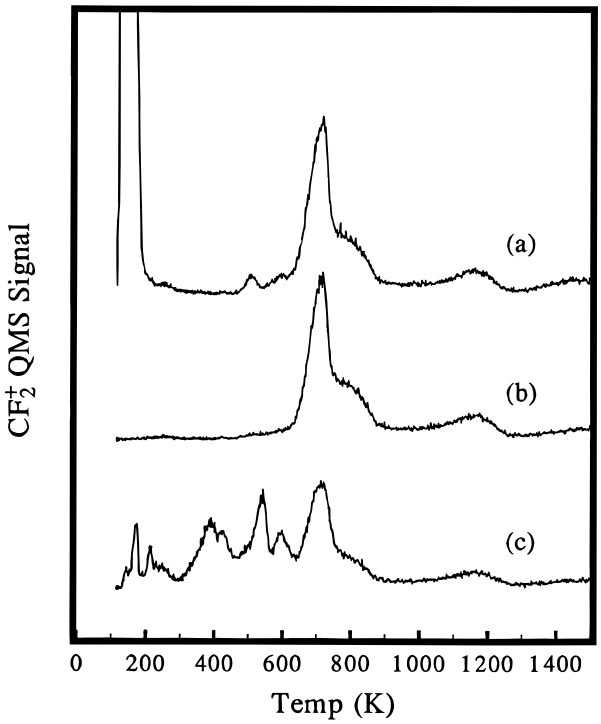

Figure 7. CF_2^+ TDS signal, from a multilayer CF_3I exposure, following: (a) CF_3I exposure at 100 K; (b) CF_3I exposure at 100 K, heating to 200 K, and 5 min low-energy electron bombardment at 100 K; (c) CF_3I exposure at 100 K, and 5 min low-energy electron bombardment at 100 K.

and positioning it in front the QMS ionizer. If this procedure is used to electron bombard the entire crystal face for an extended length of time following a multilayer CF_3I exposure, heating the crystal to 500 K results in the intermediate hexagon of Figure 6C visible over the entire crystal surface. If this same sequence is followed, except with the molecular CF_3I first removed by heating to 200 K before electron irradiation, no intermediate hexagon is observed.

TDS following electron irradiation of the multilayer yields several new features, as illustrated by the CF_2^+ TDS spectra in Figure 7. Curve a shows the normal TDS after a multilayer exposure at 100 K, with the overranged multilayer state at 136 K, CF_3 at 705 K, and CF_2 at 1165 K. The spectrum shown in curve b results from first flashing the temperature to 200 K following the CF_3I dose, cooling to 100 K, and irradiating with electrons for 5 min. Curve c results from 5 min of electron irradiation at 100 K immediately following the CF_3I exposure. Electron-induced decomposition (EID) of multilayer CF_3I is apparent, resulting in several new features between 200 and 700 K. It is interesting that the small features from curve a at 510 and 590 K seem to be enhanced in curve c, indicating that electrons from the QMS ionizer can cause a small amount of damage to the CF_3I multilayer even during a normal TDS experiment.

4. Discussion

4.1. LEED. The LEED pattern we identify most commonly following CF_3I adsorption is the $(\sqrt{3}\times\sqrt{3})R30°$ pattern shown in Figure 2D. It is seen for all exposures above 20% saturation. The disappearance of this pattern by 1100 K for all coverages coincides with the desorption of atomic iodine, as identified by TDS (Table 1). Therefore, we are led to conclude that atomic iodine created by dissociation of CF_3I is adsorbed in a $(\sqrt{3}\times\sqrt{3})R30°$ configuration. Indeed, atomic iodine is known to adopt a

$(\sqrt{3}\times\sqrt{3})R30°$ structure on other close-packed single crystal surfaces.[26,27]

The ideal coverage of the $\sqrt{3}$ structure is $^1/_3$ monolayer. However, it is improbable that saturation with CF_3I produces this coverage of I(ad). Instead, we postulate that the surface is covered with domains of $\sqrt{3}$ iodine, coexistent with areas occupied by other dissociation fragments, e.g., F(ad), C(ad), and/or CF_2(ad). The $\sqrt{3}$ superlattice appears at coverages as low as 20% of saturation. This corresponds to, at most, an absolute coverage of 0.07 monolayers suggesting that the structure is stabilized by attractive I−I interactions.

At high coverages (≥70% saturation), we also observe a (2×2) LEED pattern. Upon heating, the $^1/_2$-order spots of this pattern always split continuously to the $\sqrt{3}$ positions. This indicates that the domains of the (2×2) and $\sqrt{3}$ structures are small, and as the sample is heated, the fraction covered by $\sqrt{3}$ increases at the expense of the (2×2).[24]

The (2×2) superstructure in LEED could correspond to one of two real-space structures: a p(2×2), or three domains of a p(2×1). Both would generate the (2×2) pattern. If, however, the four corners of the unit cell are occupied by iodine atoms, as we assume for the $\sqrt{3}$ structure, then a p(2×1) adlattice would place iodine atoms in adjacent surface sites, an impossible situation given the relative sizes of I (or I^-) and Ru. We propose, therefore, that the LEED image shown in Figure 2B is due to a p(2×2) iodine adlattice.

Further, the (2×2) pattern, and the CF_3 desorption state at 705 K, are both first observed at the same CF_3I exposure (60−70% saturation). Furthermore, all evidence of the p(2×2) pattern disappears at 800 K, after desorption of CF_3, resulting in the $(\sqrt{3}\times\sqrt{3})R30°$. Hence, the (2×2) seems coupled to the existence of CF_3(ad).

We propose that each p(2×2) unit cell consists of one iodine atom and one CF_3 group. Although there is clearly not a chemical bond between them under the conditions where the (2×2) is observed,[7] there is nonetheless some type of attractive interaction which stabilizes this structure. As the CF_3 desorbs around 700 K, the p(2×2) collapses locally to a $\sqrt{3}$ structure consisting only of I(ad). This is consistent with the continuous progression of the superstructure from (2×2) to $\sqrt{3}$ upon annealing.

This model explains the progression, with *increasing* CF_3I exposure, from a $\sqrt{3}$ structure (ideal coverage of $^1/_3$), to a *less dense* p(2×2) structure (ideal coverage of $^1/_4$). The early appearance of the $\sqrt{3}$ structure is due to attractive interactions. As coverage increases, CF_3(ad) groups are stabilized, and are accommodated within a p(2×2) unit cell. According to our model, the upper limit of iodine coverage at saturation is 0.25 monolayer. As mentioned above, a saturation coverage much less than 0.33 is very plausible.

4.2. ESDIAD. The two ESDIAD features observed over the widest range of conditions in this system are the central spot and the small hexagon. The progression of these features with annealing temperature, starting from a multilayer or saturation coverage at 100 K, is shown schematically in Figure 1. The ESDIAD patterns are also correlated with the corresponding surface adsorbates[7] and with the desorption products (cf. Table 1).[2] (We do not show a corresponding figure for subsaturation coverages, since there are far less data to establish the nature of the adsorbed species there as a function of coverage and temperature.) We turn now to an identification of the two major ESDIAD features.

Normal Emission: C−F Bonds. At most temperatures and coverages, the ESDIAD images are dominated by emission of F^+ at a desorption angle normal to the surface plane. This is illustrated in Figure 3. Upon desorption of molecular CF_3I, one central beam is visible, indicating normal emission of F^+. This pattern remains unchanged until CF_3 begins to desorb at approximately 700 K. Since XPS shows that CF_3(ad) is the dominant fluorocarbon fragment present on the surface in this temperature range, the observation of a single normal emission beam has led us to conclude that CF_3(ad) groups adopt a "tilted" configuration in which one C−F bond is perpendicular to the surface plane, while a trigonal pyramidal shape is essentially retained.[7] HREELS results uphold this conclusion.[7] However, significant normal emission remains after desorption of CF_3, indicating that species other than CF_3(ad) contribute to this image as well.

Small Hexagon: Atomic Fluorine. In addition to normal emission, lobes of hexagonal symmetry are observed. Following a multilayer CF_3I exposure, we first see a small hexagonal pattern at 700 K (Figure 3), the same temperature at which XPS shows an increase in F(ad).[7] This pattern is somewhat clearer at 800 K, perhaps because the intensity of normal emission decreases with CF_3(ad) desorption. It remains until desorption of F(ad) at 1225 K. The fact that the lobes have different intensities in different areas of the surface cannot be attributed to anomalies in the sample−gun−detector system, since there are other experimental conditions and patterns where no asymmetries exist. Instead, we suspect that it is most likely associated with a slight surface misorientation and, hence, a preferential step orientation. (A miscut of ±1° is within our limits of accuracy.) Hence, we postulate that the hexagon is generated by ESD from defect sites. This is verified by Figure 6A, an ESDIAD image following CF_3I adsorption on a defect-rich surface, in which all six lobes of the hexagon are clearly visible.

As stated above, the first appearance of the small hexagon in Figure 3 coincides with significant growth of the F(ad) XPS peak, indicating that the small hexagon may be due to ESD of atomic fluorine. Further evidence is provided by the increase in CF_4 desorption, coupled with the decrease in CF_3 desorption, which results from a defect-rich surface, as shown by Figure 5. Although it is not clear exactly which carbon-containing species react to form CF_4, the reaction must involve F(ad). Hence, the presence and intensity of the CF_4 state indicate a substantial amount of C−F bond cleavage, associated with an increase in the F(ad) concentration and thus consistent with the bright hexagonal ESDIAD image seen in Figure 6A. Finally, the ESDIAD image generated by XeF_2 adsorption on the defect-rich surface (Figure 6B) is identical to that generated by CF_3I on the same surface (Figure 6A). Hence, the combined evidence indicates strongly that the small hexagonal ESDIAD pattern results from ESD of F(ad) adsorbed on defect sites. The 6-fold symmetry of this pattern suggests that the F(ad) is adsorbed along the 6-fold Ru step edges.

Using this assignment, the temperature at which the small hexagon first appears then provides information on the temperature at which C−F bond scission occurs. At low coverages, as we show in Figure 4A, features of the small hexagon are apparent following annealing to 400 K. We have previously shown that C−F bonds, most probably from CF_3(ad), break between 200 and 400 K, producing F(ad) at low coverages and possibly ejecting CF_x fragments directly into the gas phase at higher

(26) Felter, T. E.; Hubbard, A. T. *J. Electroanal. Chem.* **1979**, *100*, 473.

(27) Forstmann, F.; Berndt, W.; Buttner, P. *Phys. Rev. Lett.* **1973**, *30*, 17.

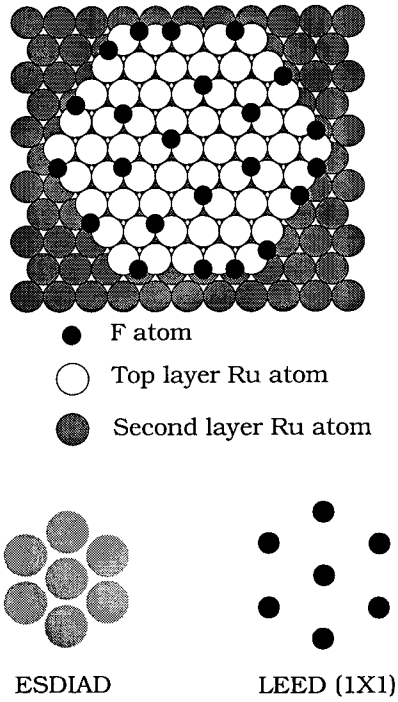

Figure 8. Adsorption sites of F(ad) on step edges and terraces of Ru(001) which could result in the small hexagonal ESDIAD image. The (1×1) LEED pattern gives the orientation of the desorbing species with respect to the substrate.

coverages.[7] The appearance of the small hexagon at 400 K from a 30% saturation exposure, along with the corresponding decrease in normal emission—presumably resulting from a loss of CF_3(ad)—supports this model. However, the ESDIAD results alone do not allow us to determine whether C−F bond scission and formation of F(ad) occur by 400 K for higher coverages. The intense normal emission in this temperature range for the high coverages overwhelms any features of the small hexagon which may exist.

This is the first firm identification of off-normal emission from atomic F, although previous work by Madey et al. suggested that such might occur on defect-rich portions of a Ru(001) crystal following exposure to NF_3.[12,28] Also, ESD-generated F^+ was detected at angles both normal and 30° off-normal from F/W(100), although no attempt was made to attribute the off-normal beam to a specific surface structure.[29] Another relevant study, concerning electron-induced defluorination of PF_3 on Ru(001),[21] did not reveal the small hexagon.

Figure 8 shows possible adsorption sites for F(ad) which would result in the observed hexagonal ESDIAD image. A comparison of the reciprocal-space (1×1) LEED pattern for the clean surface (Figure 2A) with the real-space ESDIAD image (Figure 6A) gives the desorption direction of the ESD species relative to the substrate orientation. We can see from Figure 8 that desorption of F(ad) from adsorption sites along the six step edge directions will generate the ESDIAD image we observe. These adsorption sites have somewhat arbitrarily been shown in Figure 8 as pseudobridging sites, instead of atop sites. This may not be an accurate representation, as ESD is known to be more efficient from adsorption sites of reduced coordination.[30]

Also implied by Figure 8 is the generation of an ESDIAD normal emission beam from ESD of F(ad) on terraces. Given the high electronegativity of fluorine, we expect the adsorption sites of F(ad) to be the electron-rich 3-fold hollow sites, as indicated in Figure 8. The high coordination of these adsorption sites may lead to a very low cross-section for F(ad) ESD.[30] Indeed, an investigation by Madey into the ESDIAD behavior of oxygen on stepped W(110) surfaces has shown that no ESD O^+ emission is detected from the flat terraces, while intense O^+ emission is seen in the "downstep" direction from step edges.[31] However, an ESD investigation of F^+ from W(100) detects F^+ desorbing in a direction normal to the surface plane.[29] This implies ESD of atomic fluorine from crystal terraces and leads us to believe that ESD of terrace F(ad) contributes to normal emission in this system as well.

Our results indicate that ESDIAD is much more sensitive to the detection of F(ad) than XPS. We have previously reported that XPS of CF_3I on Ru(001) detects no F(ad) above 900 K, although desorption of atomic fluorine is observed at 1226 K.[7] ESDIAD, on the other hand, identifies lobes of the small hexagon at 1200 K, which disappear by 1250 K. The sensitivity of ESD-based techniques toward fluorine detection is well-known, with limits as low as 3×10^9 atoms/cm^2 estimated for mass spectrometric detection of ESD-generated F^+.[10]

Intermediate and Large Hexagons. We observe the large hexagon, shown in Figure 4B, only at coverages below 50−60% saturation. Unlike the small hexagon, this image does not appear to be defect-related, as all six lobes are visible at all points on the surface. Furthermore, no evidence of the pattern is seen at any CF_3I coverage on the defect-rich surface. This large hexagon is never visible past 700 K, the temperature at which CF_3 desorption occurs for higher coverages. Therefore, we speculate that this large hexagon is generated by two orientations of azimuthally-fixed CF_3(ad) exhibiting C_{3v} symmetry. While we have proposed that CF_3(ad) groups at saturation coverages are adsorbed in a tilted configuration,[7] this may not be true at coverages well below saturation (<50%, where this large hexagon is observed). Instead, isolated CF_3(ad) species may adopt a C_{3v} configuration. In this model, the tilted configuration then is associated with a crowded surface layer, whereas the C_{3v} configuration is associated with a more open surface, where sites are still vacant to accept dissociation products.

It is interesting that as the CF_3I coverage increases above 60% saturation, the large hexagon may be visible, but only with increasing electron beam exposure. Once again, no evidence of this pattern is observed above 700 K, suggesting that it must still be assigned to CF_3(ad). Its electron-beam sensitivity here implies that surface fragments created by electron-induced decomposition (EID) may lead to structural changes in CF_3(ad). This is illustrated once again by the electron-beam damage experiments outlined in section 3.4. Figure 7 shows that a number of new desorption products result from EID of CF_3I multilayers. Although we have not attempted to identify these new species, it is likely that some are due to carbon−carbon coupling reactions, as seen following low-energy electron irradiation of CF_3I multilayers on Ni(100).[8]

We postulate that the intermediate hexagon in Figure 6C resulting from the electron-irradiated multilayer is also generated by CF_3(ad), since desorption of CF_3 (Figure 7) coincides with disappearance of the hexagonal pattern. Unlike the large hexagon, the intermediate hexagon forms *only* after EID of a multilayer. Thus, it seems that EID-

(28) Madey, T. E.; Polak, M.; Johnson, A. L.; Walczak, M. M. In *Desorption Induced by Electronic Transitions DIET III*; Stulen, R. H., Knotek, M. L., Eds.; Springer-Verlag: Berlin, 1987; Vol. 13; p 120.
(29) Park, C.; Kramer, M.; Bauer, E. *Surf. Sci.* **1981**, *109*, L533.
(30) Feibelman, P. J. In *Desorption Induced by Electronic Transitions DIET I*; Tolk, N. H., Traum, M. M., Tully, J. C., Madey, T. E., Eds.; Springer-Verlag: Berlin, 1983; Vol. 24; p 61.
(31) Madey, T. E. *Surf. Sci.* **1980**, *94*, 483.

created fragments alter the structure of CF_3(ad) in this case as well.

Possible Contributions of CF_2. Finally, a brief discussion of CF_2(ad) is in order. XPS indicates a significant contribution from CF_2(ad) below 700 K, but not at higher temperatures.[7] TDS shows a CF_2 desorption state at 1165 K.[2] While thermal desorption suggests that the state originates from molecular CF_2(ad)—because there are no characteristics of recombinative desorption—neither XPS nor HREELS shows any indication of C−F bonds above 700 K.[7] Hence, the nature of the high-temperature state remains questionable.

Our ESDIAD results show no special features attributable to CF_2(ad) at any temperature. A round normal emission pattern dominates at temperatures below 700 K (cf. Figure 1), where CF_2(ad) is certainly present. This points toward CF_2(ad) being adsorbed in one of two possible orientations: (1) one C−F bond is oriented perpendicular to the surface plane and contributes to the normal emission or (2) the molecular plane is oriented parallel to (or highly inclined toward) the surface plane, making ESD-generated F^+ ions undetectable. At this point we cannot conclude which of these two scenarios is correct.

The ESDIAD images observed above 700 K offer little help as only normal emission and the small hexagon are observed. These images could result from F(ad) alone, or from F(ad) with CF_2(ad). A normal emission intensity decrease is observed in moving from 1000 to 1200 K, the temperature range where CF_2 desorbs. However this may also reflect the beginning of F(ad) desorption peaked at 1226 K and, therefore, cannot be assigned to loss of perpendicularly oriented CF_2(ad).

5. Conclusions

LEED and ESDIAD have been used to study the long- and short-range structures of CF_3I, and its decomposition products, adsorbed on Ru(001). A LEED investigation following CF_3I adsorption at 100 K identifies a $(\sqrt{3}\times\sqrt{3})R30°$ surface structure, for CF_3I exposures as low as 20% saturation. By analogy with other studies of iodine adsorption, this probably reflects a primitive $\sqrt{3}$ unit cell of atomic iodine, ideal coverage = $^1/_3$. The low exposure at which this pattern first appears indicates island formation. As the CF_3I exposure increases to a level where CF_3 desorption (at 705 K) begins, a new LEED pattern showing $^1/_2$-order spots is visible. This pattern is attributed to iodine atoms adsorbed in a p(2×2) surface structure. With heating, this p(2×2) pattern begins to split, eventually disappearing with desorption of CF_3(ad). Less surface crowding following CF_3 desorption allows iodine atoms to once again adopt the $\sqrt{3}$ structure. We postulate that CF_3 groups are adsorbed in the center of the p(2×2) unit cell.

ESDIAD of CF_3I on Ru(001) shows a variety of images which provide information about the reactions which occur on the surface, as well as the structure of the products which result from these reactions. A central spot, resulting from desorption of F^+ normal to the surface plane, is the dominant image at most coverages and temperatures. This indicates that CF_3(ad) groups are bonded to the surface in a "tilted" configuration with one C−F bond oriented perpendicular to the surface plane.

As the crystal temperature is raised, lobes of a small hexagon emerge from beneath the normal emission spot. Adsorption of CF_3I and XeF_2 on defect-rich surfaces clearly shows all six lobes of this small hexagon, indicating it is generated by atomic fluorine adsorbed on step and defect sites. The persistence of this pattern to 1200 K (where the last atomic fluorine desorbs) proves that, in this case, ESDIAD and TDS are much more sensitive to the presence of F(ad) than is XPS.

Two other hexagonal patterns are visible with ESDIAD. The first is a large hexagon which disappears by 700 K, the same temperature at which CF_3 desorbs at high coverages. This correlation suggests that the pattern is generated by two orientations of CF_3(ad), each with C_{3v} symmetry. This pattern is thermally-induced at low coverages (<50% saturation) and electron-beam-assisted at higher coverages.

The remaining hexagon is intermediate in size and appears only after a multilayer undergoes electron-induced decomposition (EID). It may be that EID fragments cause CF_3(ad) to adopt a new adsorption structure which generates the intermediate hexagon.

Acknowledgment. This work is supported primarily by Ames Laboratory, which is operated for the U.S. Department of Energy by Iowa State University under Contract No. W-7405-Eng-82. In addition, the work is supported by a Graduate Assistantship in Areas of National Need (GAANN) Fellowship from the Department of Education (M.B.J.).

LA950211V